Bull. Mater. Sci. (2019) 42:158
https://doi.org/10.1007/s12034-019-1842-0

Enhanced photocatalytic activity of SnO_2 NPs by chromium (Cr) concentration

TAYEBEH KARIMI[1,2] and AZADEH HAGHIGHATZADEH[2,*]
[1]Department of Physics, Khuzestan Science and Research Branch, Islamic Azad University, Ahvaz, Iran
[2]Department of Physics, Ahvaz Branch, Islamic Azad University, Ahvaz, Iran
*Author for correspondence (haghighatzadeh@gmail.com)

MS received 27 February 2018; accepted 31 December 2018; published online 14 May 2019

Abstract. This study reports the synthesis of un- and chromium (Cr)-doped tin dioxide (SnO_2) nanoparticles (NPs) through chemical precipitation and their application for photodegradation of methylene blue dye. The obtained NPs were characterized by X-ray diffraction (XRD) analysis, transmission electron microscopy (TEM), Fourier transform infrared (FT-IR) spectroscopy, elemental mapping and ultraviolet–visible (UV–Vis) spectroscopy. The TEM and XRD results demonstrated that the SnO_2 NPs are spherical and contain polycrystalline tetragonal crystals. UV–Vis spectra showed that increasing the concentration of the Cr dopant enhances the light absorption potential of the SnO_2 NPs. Finally, the findings of the photocatalytic experiments performed for 120 min in ultraviolet irradiation under ambient conditions revealed an improvement in the degradation efficiency of the SnO_2 NPs by Cr doping.

Keywords. SnO_2 NPs; Cr concentration; chemical precipitation; optical properties; methylene blue degradation.

1. Introduction

Environmental pollution is an issue that has threatened human life and the future of many living species. In this regard, several studies have been conducted on the treatment of environmental pollutants such as organic dyes through the introduction and application of different methods [1,2]. One of the proposed methods is photocatalytic degradation of the chemical dyes that are often found in the wastewaters of chemical industries. Usually, semiconductor materials are employed for this purpose since most of them are non-toxic and environmentally friendly, they can degrade chemical dyes under light irradiation and convert them into less hazardous compounds [3,4].

Among different semiconductor materials, oxide compounds are of specific importance for photocatalytic degradation purposes [5]. For instance, nanostructured tin dioxide (SnO_2) particles have been widely considered for photocatalytic degradation of chemical dyes. This material is a compound from the IV and VI-A groups of the periodic table and is an n-type semiconductor with a band gap energy of about 3.62 eV [6]. In addition to photocatalytic degradation of environmental pollutants [7], the specific properties of SnO_2 nanostructures have represented them as appropriate candidates for a wide range of applications related to magnetic, health and biological sciences [8,9], lithium-ion batteries [10,11], gas, optical and humidity sensing [12–17], supercapacitance [18,19], photovoltaic cells [20,21] and hydrogen storage [22]. The efficiency of SnO_2 nanostructures for these applications can be improved by engineering their energy band gap. In this way, a wider and more suitable range of light absorption can be obtained to enhance the photocatalytic degradation of organic compounds. Like any other semiconductor materials, the band gap energy of SnO_2 can be engineered through doping of suitable elements. From a microscopic perspective, dopants create new electronic states in the electronic band structure of SnO_2, accelerate the production of charge carriers, increase the oxidation potential of SnO_2 and improve the degradation of chemical dyes. Heavy metal dopants such as chromium (Cr) can enhance the removal rate of dye degradation by SnO_2 nanostructures. They enhance the separation efficiency of photo-induced electrons and holes and, at the same time, they enhance the visible light absorption due to shortening of the energy band gap. Heavy metal dopants have been used for different oxide semiconductors, leading to enhanced degradation of various organic dyes [23–27].

So far, various elements have been used as dopants to improve the photocatalytic properties of SnO_2 nanostructures [28–30]. For example, Reddy *et al* [31] investigated the effect of the Cr dopant on the optical and photocatalytic properties of SnO_2 quantum dots (QDs). Their X-ray diffraction (XRD) and X-ray photoelectron spectroscopy (XPS) results approved the formation of the polycrystalline tetragonal phase of SnO_2 and Cr incorporation into the crystalline lattice of the QDs *via* bonding with oxygen, respectively. Their optical studies indicated that Cr incorporation increases the absorption intensity and the optical energy band gap of SnO_2 QDs. They reported that the observed increase in the optical energy band gap could be related to the decreased size of the SnO_2 QDs with

the addition of Cr. Also, they applied the un- and Cr-doped SnO_2 QDs to UV-based photocatalytic degradation of methyl orange. Their results showed an improvement in the degradation efficiency of the SnO_2 QDs by adding the Cr dopant and increasing the Cr concentration. They stated that this improvement can be due to the promoted recombination of the charge carriers, i.e. electrons and holes. With respect to the findings of Reddy *et al* [31] and the lack of any report about photocatalytic degradation of methylene blue (MB) by Cr-doped SnO_2 nanostructures, we synthesized SnO_2 nanostructures *via* a simple and cost-effective chemical method and added the Cr dopant to study the optical and photocatalytic behaviour of the Cr-doped samples. The main advantage of the precursor materials utilized for the synthesis of the SnO_2 nanostructures is that they are more cost-effective, eco-friendly and low-risk compared to those required for many other metal oxides including TiO_2, which are usually prepared using the toxic and high-risk precursors of titanium (IV) fluoride, titanium (IV) chloride, titanium (IV) butoxide and titanium (IV) isopropoxide [32,33].

2. Experimental

First, 0.9 g $SnCl_2{\cdot}2H_2O$ (Merck, 99.99%) was added to 40 ml ethanol. Then, 1 ml ammonia was added to the solution and was stirred to precipitate the Sn^{2+} ions in the form of $Sn(OH)_2$. The result was a milky-like solution. After this, the precipitated particles were centrifuged and dried for 24 h in an oven at 80°C. In the next step, an annealing process was carried out for 2 h at 550°C in a box furnace under an ordinary atmosphere to obtain a white SnO_2 powder. For the preparation of the Cr-doped samples, a specified amount of $CrCl_2{\cdot}6H_2O$ (Merck, 99.99%) (table 1) was added to the Sn^{2+} solution and the described procedure was repeated. Each sample was addressed with the name presented in table 1.

The crystalline structure of the obtained powders was studied by an XRD Seifert ID 3003 system that was equipped with a copper anode with the excitation wavelength of 1.5406 Å. The morphology of the samples was probed by transmission electron microscopy (TEM; CM120, Philips). An elemental mapping detector attached to a scanning electron microscope (SEM; TeScan, Mira 3-XMU) was used to analyse the elemental composition of the samples. The particle size histograms of the samples were plotted with the help of the Digimizer and Origin programs. Fourier transform infrared (FT-IR) spectroscopy was carried out by using a Perkin-Elmer System 2000 instrument over the range of 400–4000 cm^{-1}. Also, the ultraviolet–visible (UV–Vis) (absorption and reflection) spectra of the samples (in the form of a film) were recorded by using a Hatch DR 5000 UV–Vis spectrometer to study their optical properties. For this purpose, a suitable amount of powder from each sample was placed on the lamella using double-sided adhesion.

Photocatalytic experiments using un- and Cr-doped samples were performed at room temperature to degrade the MB dye under UV irradiation. For each photocatalytic test, 0.01 g MB was dissolved in 100 ml deionized water. Then, 0.15 g of the prepared SnO_2 powder was added to the MB solution and mixed using a stirrer to achieve a uniform solution. The solution was exposed to UV rays and a portion of the solution was sampled for 30 min, centrifuged and its absorption spectrum was recorded by the UV–Vis spectrometer. This process was repeated for the Cr-doped samples, as well.

Table 1. Amount of specified concentration for preparing samples and the name used for each of them.

Sample name	Dopant (Cr) concentration (%)	Material
Cr0	0	Un-doped SnO_2
Cr1	5	Cr-doped SnO_2
Cr2	8	Cr-doped SnO_2
Cr3	11	Cr-doped SnO_2

3. Results and discussion

To assess phase purity of the obtained materials and evaluate their crystalline structures, XRD analysis was utilized. The obtained results (figure 1) show that all samples are crystalline and their diffraction peaks match the standard card of bulk tetragonal SnO_2 (JCPDS Card No. 01-070-4177) [34]. Also, the results exhibit that adding a minimum concentration of the dopant increases the intensity of the diffraction peaks up to a maximum intensity. However, after the addition of a certain amount of Cr, increasing the Cr concentration decreases the intensity of the diffraction peaks. In addition, full width at half maximum (FWHM) and the distance between the crystalline planes of SnO_2 are decreased by increasing the Cr concentration. Furthermore, the positions of the diffraction peaks shifted toward greater angles upon doping due to the lower ionic radii of Cr compared with Sn [35]. This observation implies that the incorporation of Cr into the lattice

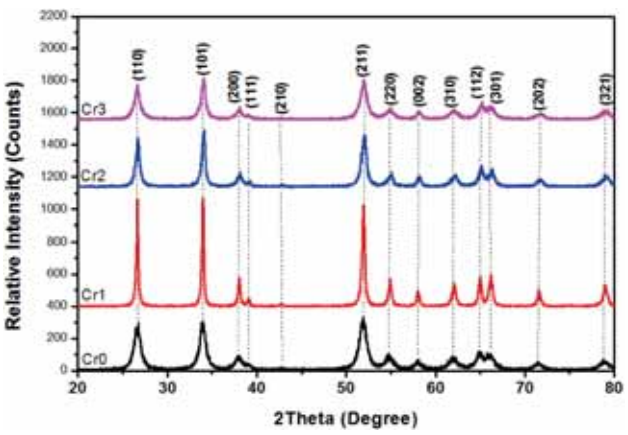

Figure 1. XRD patterns of un- and Cr-doped SnO_2 samples.

Table 2. Lattice constant of un- and Cr-doped SnO_2 samples.

Sample name	$a = b$ (A)	c (A)
Cr0	4.76307	3.16710
Cr1	4.72630	3.18826
Cr2	4.71174	3.14330
Cr3	4.72673	3.15842

structure of SnO_2 introduces strain to the crystal lattice and induces some changes in the crystal parameters of SnO_2. Similar observations were reported about doping SnO_2 structures with the Cr and Fe ions [36,37].

To calculate the crystallite size of the un- and Cr-doped SnO_2 samples, the Scherrer equation (equation (1)) [38] was used since it is valid for the following cases FWHM $\times$ cos $\theta = 1$. In the Scherrer equation,

$$D = \frac{0.94\lambda}{\beta \cos\theta} \tag{1}$$

D is the crystallite size, λ is the applied X-ray wavelength, β is the FWHM and θ is the position of the diffraction peak. Based on this equation, the crystallite sizes of the Cr0, Cr1, Cr2 and Cr3 samples are equal to 27.85, 42.29, 27.44 and 23.37 nm, respectively.

The lattice constant of samples was calculated in order to estimate the effect of addition of Cr in the crystalline lattice of SnO_2, using equation (2) and characteristics of dominate diffraction peaks.

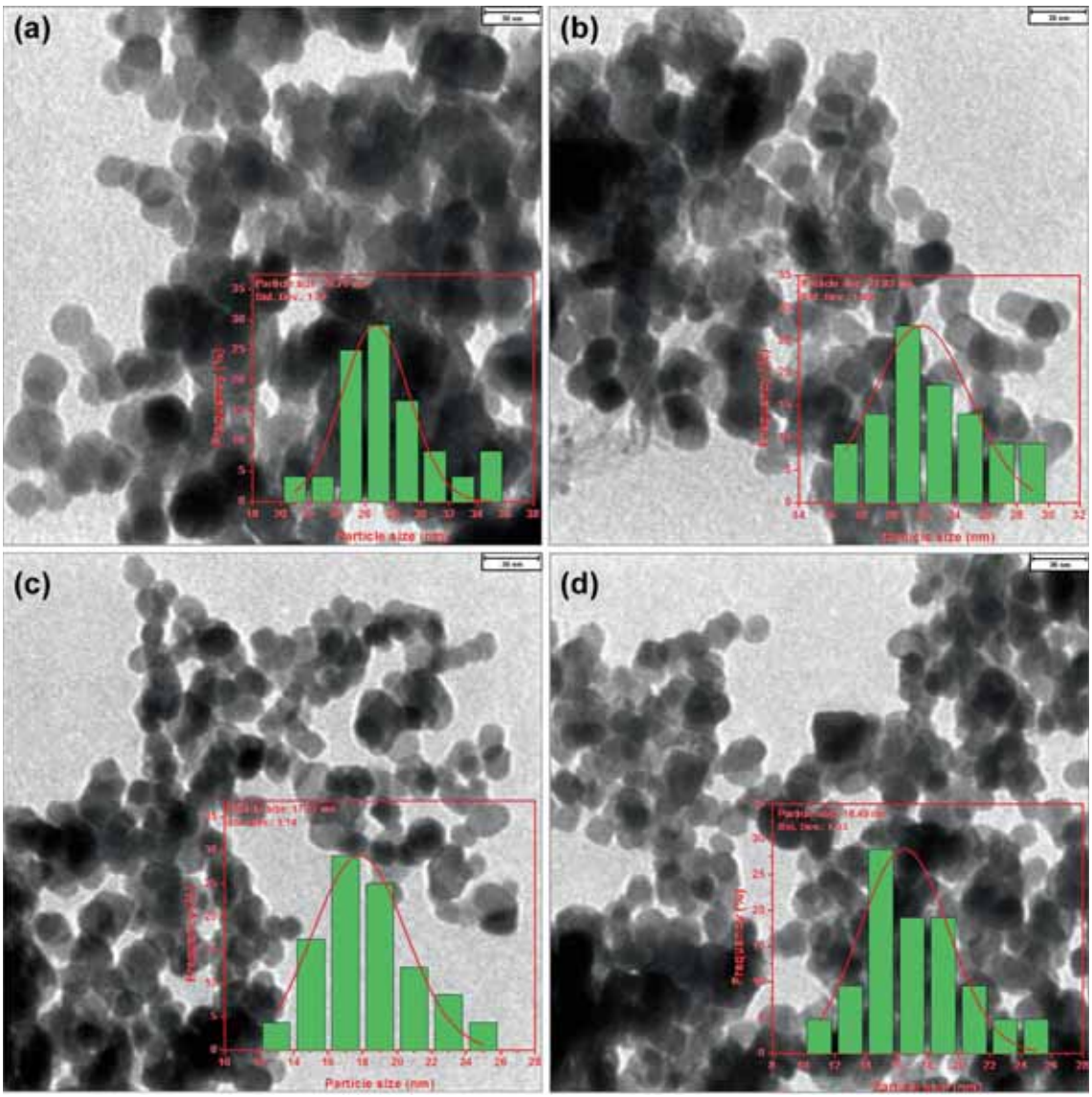

Figure 2. TEM images of (**a**) Cr0, (**b**) Cr1, (**c**) Cr2 and (**d**) Cr3 samples. The inset in each image presented the particle size histogram of SnO_2 NPs.

$$\frac{1}{d^2} = \frac{h^2 + k^2}{a^2} + \frac{l^2}{c^2} \quad (2)$$

where d is the distance between crystalline planes, h, k and l are Miller indices and a and c are lattice constants. The obtained results (table 2) indicated some decreases in lattice constants after addition of Cr, which can be related to the lower ionic radii of Cr compared with Sn and induced strain in the crystalline lattice of SnO_2 [36,37].

Figure 2 presents the TEM images and particle size histograms of the un- and Cr-doped SnO_2 samples. As figure 2a displays, the un-doped sample contains spherical-like particles with the mean particle size of 26.76 nm. In comparison, figures 2b and c shows that Cr addition does not change the morphology of SnO_2 but decreases its particle size. In general, the TEM results show that the sizes of all SnO_2 structures are smaller than 100 nm. Therefore, the samples can be named as un- and Cr-doped SnO_2 nanoparticles (NPs). The reason for the decreased size of the SnO_2 NPs might be the growth mechanism of the particles due to the effect of dopant nucleation on the growth of metal oxide semiconductors. As the TEM results suggest, dopant concentration plays a key role in varying the size of semiconducting nanomaterials. The dependency of the SnO_2 particle size on dopant concentration can be related to the variations in the amount and the rate of supersaturation, colloidal stability and re-crystallization caused by dopant addition. Among these three factors, supersaturation has a more deterministic role since it strongly depends on the dopant element [39].

The contribution of supersaturation to the particle growth process can be investigated according to the concept of Gibbs free energy. Based on this concept, all thermodynamic

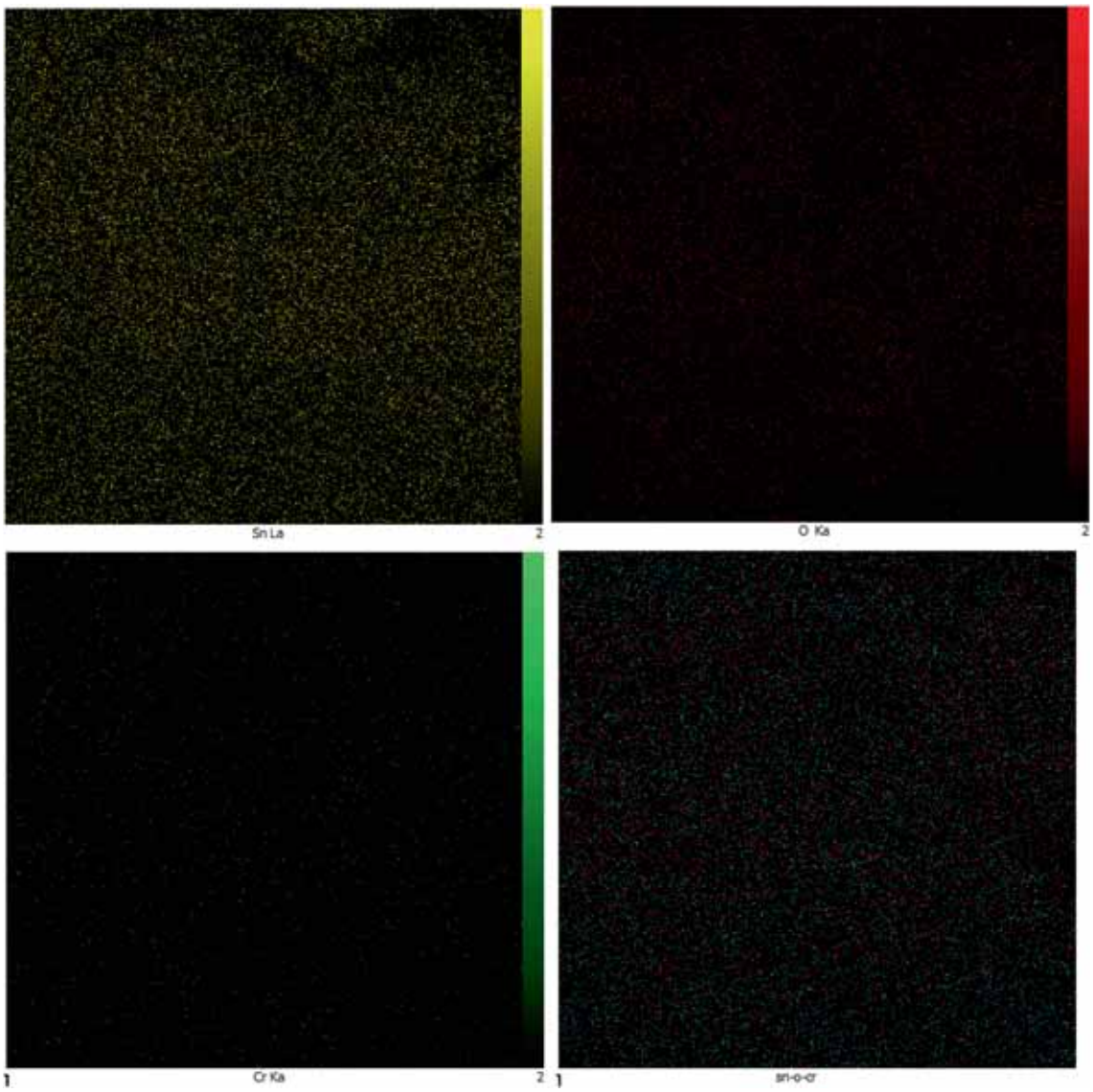

Figure 3. Elemental mapping of Cr1 sample.

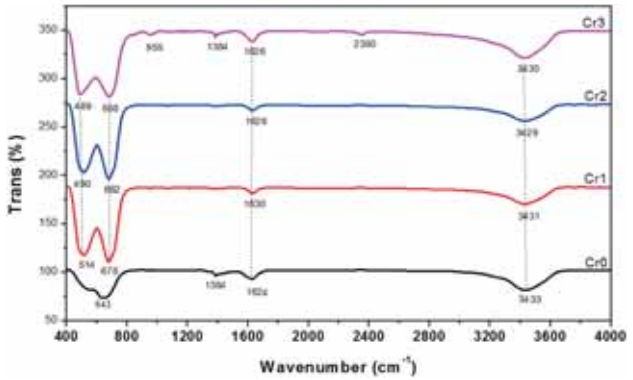

Figure 4. FT-IR spectra of un- and Cr-doped SnO_2 NPs.

systems tend to reach a lower level of energy due to the compulsory nature of nucleation and growth. In the absence of any dopant, the formed nuclei are larger in size due to the lower level of Gibbs free energy. However, when the concentration of the dopant increases, the level of Gibbs free energy elevates, leading to the reduced size of the generated nuclei. It also enhances the solubility of the particles in the system and reduces supersaturation. Meanwhile, decreased supersaturation results in a decreased particle size [40].

An elemental mapping method was adopted as a simple and valid approach to confirm the presence of the desired elements and assess the quality of the samples. The elemental map of Cr1 is presented in figure 3 but the elemental maps of the other samples are not reported. As figure 3 exhibits, the Cr1 sample is composed of uniformly distributed Sn, O and Cr elements.

FT-IR spectroscopy was used to qualitatively and quantitatively study the chemical structure of the un- and Cr-doped SnO_2 NPs. The obtained FT-IR spectra (figure 4) outline two common transmission bands for all samples. These bands are located over the frequency ranges of 1624–1630 cm^{-1} and 3429–3433 cm^{-1} and are related to the bending vibrational mode of O–H [41,42]. For the un-doped sample, the transmission bands appeared at about 643 and 1384 cm^{-1} can be attributed to the O–Sn–O and C–H vibrations, respectively [43,44]. The 1384 cm^{-1} band has also appeared in the spectra of the Cr2 and Cr3 samples. For all Cr-doped samples, a transmission band has emerged over the range of 489–514 cm^{-1} that corresponds to the vibration of the Cr–O bond [45]. In the case of Cr3, a vibrational band can be seen at 953 to 955 cm^{-1}, which are related to the bending vibration of Cr=O=Cr [46]. Overall, the FT-IR results are in agreement with the XRD results and verify the incorporation of Cr into the crystalline lattice of the SnO_2 NPs.

The absorption spectra of the un- and Cr-doped SnO_2 NPs are depicted in figure 5a. As can be observed, all SnO_2 samples contain an absorption edge at 250 to 350 nm, in line with previous reports. Moreover, the Cr-doped SnO_2 NPs possess a second absorption edge in the range of 540–650 nm. The presence of this absorption edge is associated with the formation of the chromium oxide (Cr_xO_y) partial phase due to the

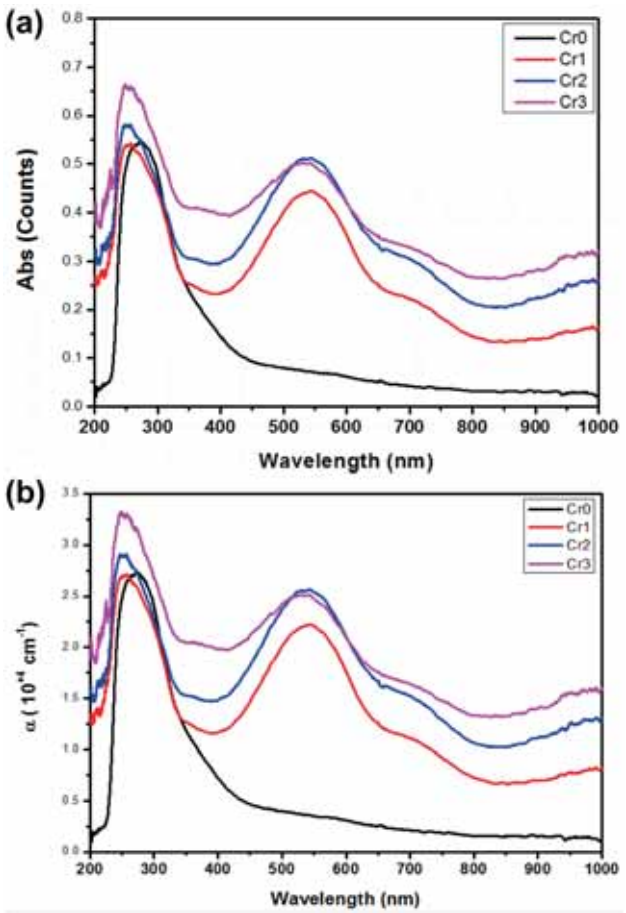

Figure 5. (**a**) Absorption and (**b**) absorption coefficient spectra of un- and Cr-doped SnO_2 NPs.

incorporation of Cr atoms into the crystalline lattice of SnO_2. Also, the absorption spectra indicate that increasing the concentration of Cr intensifies the absorption of the SnO_2 NPs, which can be considered as a hallmark of the enhanced optical efficiency for photocatalytic dye degradation. Using reflection (R) and transmission (T) spectra ($A = -\log T$) which are not shown here, and based on equation (3), the absorption coefficient (α) of SnO_2 nanostructures can be obtained as follows [47–49]:

$$\alpha = \frac{1}{d}\ln\left(\frac{1-R^2}{T}\right), \tag{3}$$

where d is the film thickness. The obtained results (figure 5b) demonstrate an increase in α of SnO_2 nanostructures upon addition of Cr. Although there are several methods for the estimation of the optical energy band gap of semiconducting NPs, Tauc plot is the most commonly adopted method. The basis of this method is the Kubelka–Munk theory, according to which the relationship between the absorption and optical energy band gap can be described by equation (4) [50]

$$(\alpha h\nu)^n = A\left(h\nu - E_g\right), \tag{4}$$

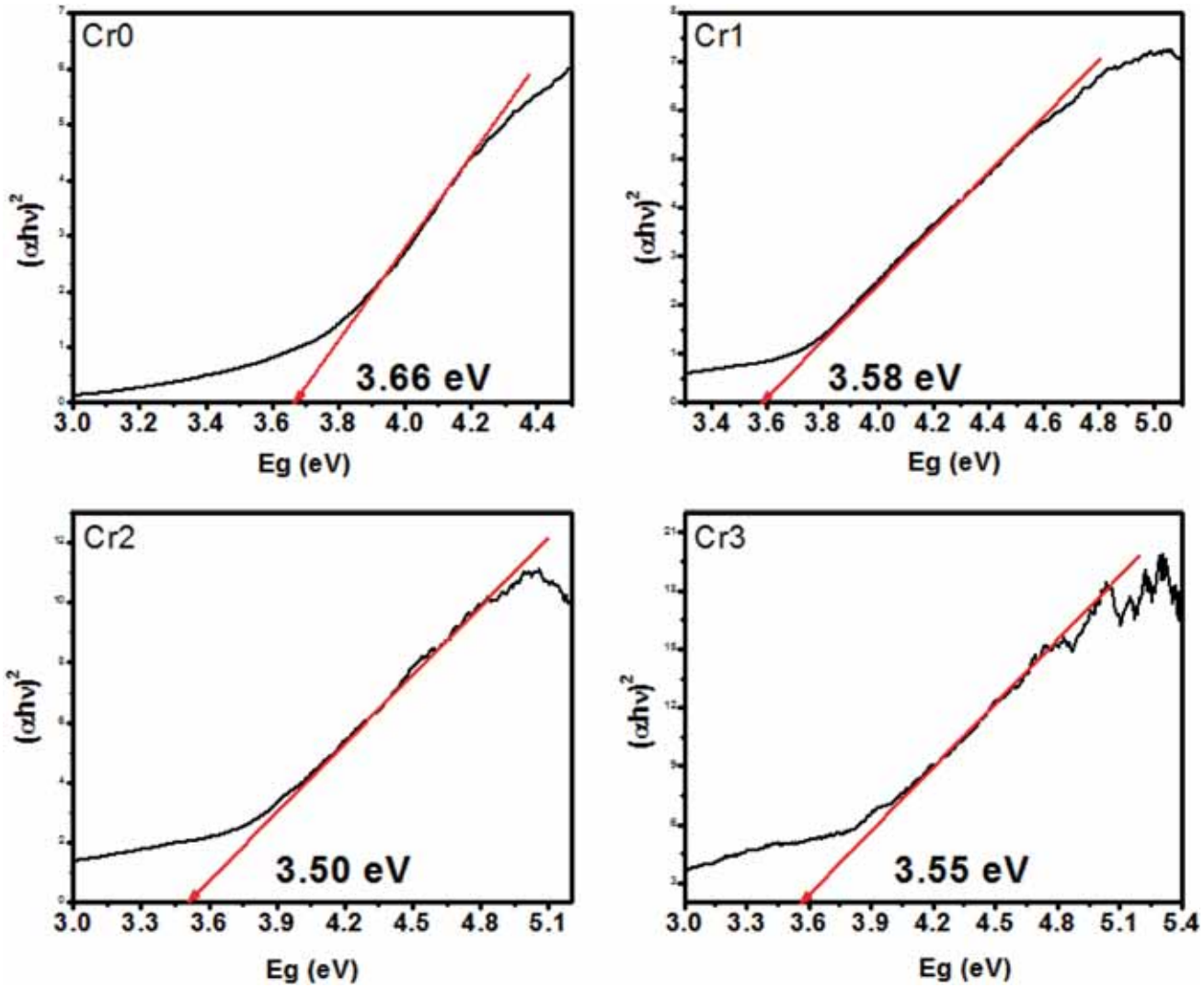

Figure 6. Tauc plots of un- and Cr-doped SnO_2 NPs.

where h is the Plank's constant, ν is the frequency, A is a constant, E_g refers to the optical energy band gap and n is a characteristic of the transition process. The acquired Tauc plots (figure 6) show a decrease in the optical band gap of the SnO_2 NPs by increasing the concentration of Cr. As mentioned about the absorption spectra, the decrease in the band gap can be ascribed to the formation of partial Cr_xO_y phases with the lower optical energy band gap compared with SnO_2 [51]. Such a decrease in the optical energy band gap for Cr-doped SnO_2 nanostructures has also been reported by other researchers [52,53] and can be interpreted using equation (5) [54]

$$E_g\,(Sn_{1-x}Cr_xO_2) = (1-x) \times E_g\,(SnO_2) + x \times E_g\,(Cr_xO_y). \quad (5)$$

Figures 7 and 8 respectively illustrate the absorption spectra and the logarithmic rate [55,56] plots of MB degradation by the un- and Cr-doped SnO_2 NPs at different intervals of UV irradiation. According to these figures, Cr doping improves the degradation efficiency of the SnO_2 NPs. Furthermore, applying higher Cr concentrations results in a greater extent of enhancement. The observed activity promotion can be related to the decrease in the particle size, which increases the surface to volume ratio based on the TEM images and intensifies absorption of the SnO_2 NPs according to the UV–Vis spectra.

During photocatalytic degradation of chemical dyes by semiconductor NPs, such as SnO_2, the NPs are optically excited. As a result, electrons of their valence band excite and transit to their conduction band. During this transition process, the electrons release and introduce the generation of free radicals in the solution. The photogenerated free radicals act as strong oxidizing agents for the degradation of chemical dyes, such as MB. These processes are described in equations (6–10) and in figure 9 [57–59]. The effectiveness of such process depends on different factors including size, optical absorption, optical band gap, morphology, the degree

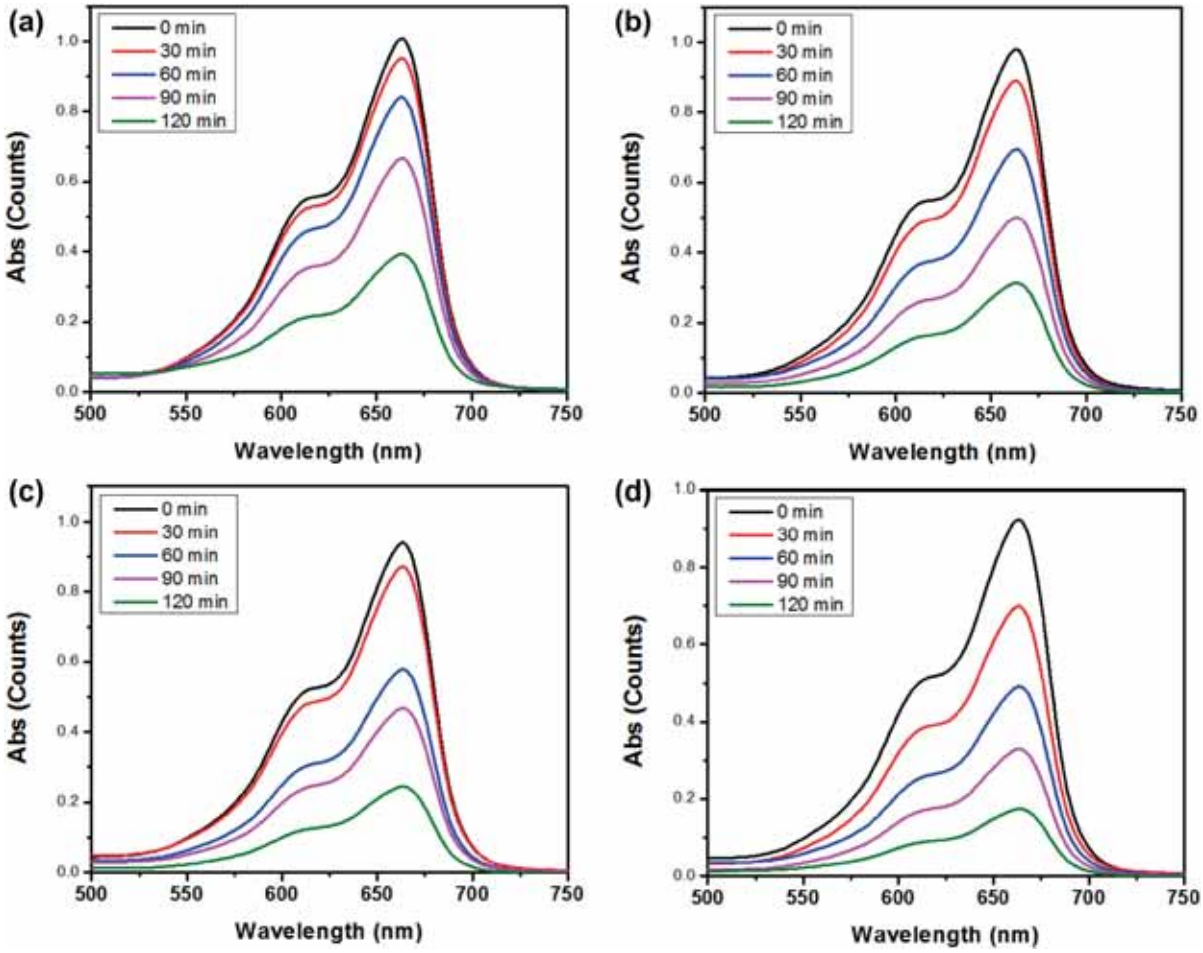

Figure 7. Absorption spectra of SnO_2 NPs after degradation of MB at different times under UV radiation for (**a**) Cr0, (**b**) Cr1, (**c**) Cr2 and (**d**) Cr3 samples.

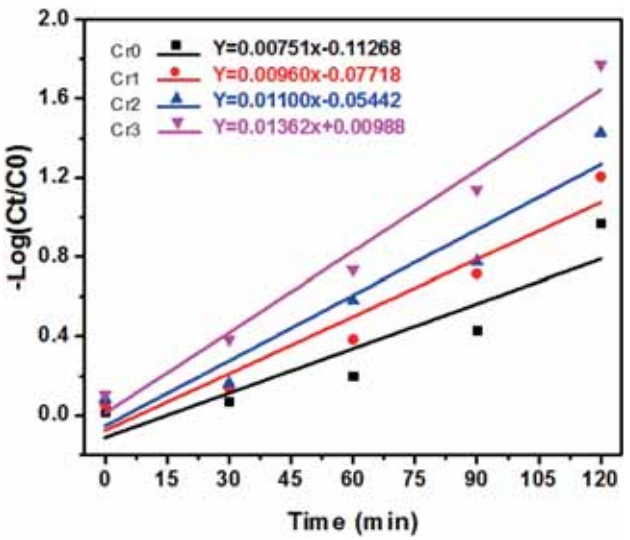

Figure 8. Degradation rate of MB for un- and Cr-doped SnO_2 NPs at different times under UV radiation.

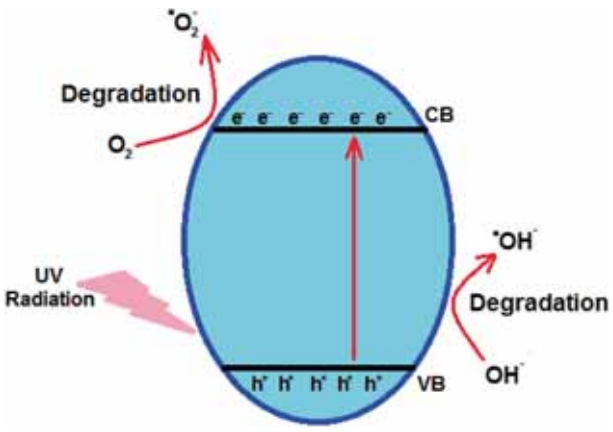

Figure 9. Schematic diagram of MB degradation using un- and Cr-doped SnO_2 NPs under UV radiation.

of crystallinity and the presence of crystal defects in catalyst particles [50,60,61].

$$h\nu + SnO_2 \rightarrow e^- (CB) + h^+ (VB) \quad (6)$$

$$e^- + O_2 \rightarrow {}^{\bullet}O_2^- \quad (7)$$

$$h^+ + OH^- \rightarrow {}^{\bullet}OH \quad (8)$$

$${}^{\bullet}O_2^- + \text{organic dyes} \rightarrow \text{degradation products} \quad (9)$$

$${}^{\bullet}OH + \text{organic dyes} \rightarrow \text{degradation products} \quad (10)$$

4. Conclusion

In this research, SnO_2 NPs were grown using a chemical precipitation method to investigate the effect of the Cr dopant on the optical and photocatalytic properties of SnO_2. The XRD results revealed the formation of polycrystalline and tetragonal SnO_2 phases. Also, they showed that Cr doping decreases the crystallite size of the SnO_2 NPs. The TEM images indicated that spherical-like SnO_2 NPs are grown and the incorporation of Cr decreases the mean particle size of the NPs. The FT-IR spectra presented the existence of bonding between Sn and O and, also, Cr and O, and confirmed the incorporation of Cr atoms into the crystal lattice of the SnO_2 NPs. The optical studies demonstrated that higher Cr concentrations respectively increase and decrease the optical absorption and optical energy band gap of the SnO_2 NPs. Finally, the results of the conducted photocatalytic experiments showed the key roles of higher absorption potential and increased the surface to volume ratio, caused by the addition of the Cr dopant in enhancing the efficiency of the SnO_2 NPs for degradation of MB dyes.

Acknowledgements

The authors would like to appreciate Islamic Azad University, Ahvaz Branch, Ahvaz, Iran for financial and instrumentational support.

References

[1] Cheraghizade M, Jamali-Sheini F and Yousefi R 2017 *Appl. Phys. A* **123** 390
[2] Schneider J, Matsuoka M, Takeuchi M, Zhang J, Horiuchi Y, Anpo M *et al* 2014 *Chem. Rev.* **114** 9919
[3] Yousefi R, Azimi H R, Mahmoudian M R and Cheraghizade M 2018 *Adv. Powder Technol.* **29** 78
[4] Mary Jacob N, Madras G, Kottam N and Thomas T 2014 *Ind. Eng. Chem. Res.* **53** 5895
[5] Cai Q and Hu J 2017 *J. Ha. Mater.* **323** 527
[6] Gu F, Wang S F, Lü M K, Zhou G J, Xu D and Yuan D R 2004 *J. Phys. Chem. B* **108** 8119
[7] Shi L and Lin H 2010 *Langmuir* **26** 18718
[8] Nguyen Hoa H, Joe S, Prellier W and Awatef H 2005 *J. Phys. Condens. Matter* **17** 1697
[9] Aquino J C R, Aragón F H, Coaquira J A H, Gratens X, Chitta V A, Gonzales I *et al* 2017 *J. Phys. Chem. C* **121** 21670
[10] Chen Jun S and Lou Xiong W 2013 *Small* **9** 1877
[11] Park M-S, Wang G-X, Kang Y-M, Wexler D, Dou S-X and Liu H-K 2007 *Angew. Chem. Int. Ed.* **46** 750
[12] Gyger F, Hübner M, Feldmann C, Barsan N and Weimar U 2010 *Chem. Mater.* **22** 4821
[13] Wongchoosuk C, Wisitsoraat A, Tuantranont A and Kerdcharoen T 2010 *Sens. Actuators B Chem.* **147** 392
[14] Li X, Gao C, Duan H, Lu B, Wang Y, Chen L *et al* 2012 *Small* **9** 2005
[15] Paulowicz I, Hrkac V, Kaps S, Cretu V, Lupan O, Braniste T *et al* 2015 *Adv. Electron. Mater.* **1** 1500081
[16] Tawale J S, Gupta G, Mohan A, Kumar A and Srivastava A K 2014 *Sens. Actuators B Chem.* **201** 369
[17] Tomer V K and Duhan S 2016 *Sens. Actuators B Chem.* **223** 750
[18] Lim S P, Huang N M and Lim H N 2013 *Cer. Int.* **39** 6647
[19] Liu Y, Jiao Y, Zhang Z, Qu F, Umar A and Wu X 2014 *ACS Appl. Mater. Interfaces* **6** 2174
[20] Ahn Sung H, Kim Dong J, Chi Won S and Kim Jong H 2013 *Adv. Mater.* **25** 4893
[21] Pang H, Yang H, Guo C X and Li C M 2012 *ACS Appl. Mater. Interfaces* **4** 6261
[22] Wang Z, Wang F, Li M, Zubair Iqbal M, Javed Q-U-A, Lu Y *et al* 2014 *Mater. Lett.* **119** 36
[23] Kyung H, Lee J and Choi W 2005 *Environ. Sci. Technol.* **39** 2376
[24] Nitoi I, Oancea P, Raileanu M, Crisan M, Constantin L and Cristea I 2015 *J. Ind. Eng. Chem.* **21** 677
[25] Pezhman M, Mohsen C and Ramin Y 2019 *Mater. Res. Express* **6** 025051
[26] Yousefi R, Jamali-Sheini F, Cheraghizade M and Zaman L 2016 *Mater. Res. Innov.* **20** 121
[27] Trindade T N S and Silva L A 2018 *J. Alloy. Compd.* **735** 400
[28] Jia T, Wang W, Long F, Fu Z, Wang H and Zhang Q 2009 *J. Phys. Chem. C* **113** 9071
[29] Al-Hamdi A M, Sillanpää M and Dutta J 2014 *J. Mater. Sci.* **49** 5151
[30] Kumar V, Govind A and Nagarajan R 2011 *Inorg. Chem.* **50** 5637
[31] Reddy C V, Babu B and Shim J 2017 *Mater. Sci. Eng. B* **223** 131
[32] Gordon T R, Cargnello M, Paik T, Mangolini F, Weber R T, Fornasiero P *et al* 2012 *J. Am. Chem. Soc.* **134** 6751
[33] Wu Hao B, Hng Huey H and Lou Xiong W 2012 *Adv. Mater.* **24** 2567
[34] ICCD P D F 1997 *Powder Diffraction File*, Newtown Square, Pennsylvania, USA
[35] Ramin Y, Mohsen C, Farid J-S, Mahmoudian M R, Abdolhossein S and Nay Ming H 2014 *Chin. Phys. B* **23** 108101
[36] Rani S, Roy S C, Karar N and Bhatnagar M C 2007 *Solid State Commun.* **141** 214
[37] Zhang L, Ge S, Zuo Y, Wang J and Qi J 2010 *Scr. Mater.* **63** 953
[38] Kafashan H, Jamali-Sheini F, Azizieh M, Balak Z, Cheraghizade M and Nasiri Vatan H 2017 *J. Alloy. Compd.* **694** 1338

[39] Guozhong C 2004 *Nanostructures and nanomaterials: synthesis, properties and applications* (London: Imperial College Press)
[40] Singh R C, Singh M P, Singh O and Chandi P S 2009 *Sens. Actuators B Chem.* **143** 226
[41] Ávila H A and Rodríguez-Páez J E 2009 *J. Non-Cryst. Solids* **355** 885
[42] Fang Z, Assaaoudi H, Lin H, Wang X, Butler I S and Kozinski J A 2007 *J. Nano. Res.* **9** 683
[43] Wang X, Qiu S, Liu J, He C, Lu G and Liu W 2014 *Eur. J. Inorg. Chem.* **2014** 863
[44] Dong Y, Zhao Z, Wang Z, Liu Y, Wang X and Qiu J 2015 *ACS Appl. Mater. Interfaces* **7** 2444
[45] Nilavazhagan S, Muthukumaran S and Ashokkumar M 2013 *J. Mater. Sci. Mater. Electron.* **24** 2581
[46] Zapata P M C, Nazzarro M S, Parentis M L, Gonzo E E and Bonini N A 2013 *Chem. Eng. Sci.* **101** 374
[47] Benouis C E, Benhaliliba M, Mouffak Z, Avila-Garcia A, Tiburcio-Silver A, Ortega Lopez M *et al* 2014 *J. Alloy. Compd.* **603** 213
[48] Benhaliliba M, Benouis C E, Aida M S, Yakuphanoglu F and Sanchez Juarez A 2010 *J. Sol-Gel Sci. Technol.* **55** 335
[49] Adelifard M, Eshghi H and Mohagheghi M M B 2012 *Appl. Surf. Sci.* **258** 5733
[50] Jamali-Sheini F, Yousefi R, Ali Bakr N, Cheraghizade M, Sookhakian M and Huang N M 2015 *Mater. Sci. Semicon. Proc.* **32** 172
[51] Biswas S 2018 *J. Mol. Model.* **24** 111
[52] Gandhi T I, Ramesh Babu R and Ramamurthi K 2013 *Mater. Sci. Semicon. Proc.* **16** 472
[53] Ibrahim N B, Abdi M H, Abdullah M H and Baqiah H 2013 *Appl. Surf. Sci.* **271** 260
[54] Jamali-Sheini F, Cheraghizade M, Niknia F and Yousefi R 2016 *MRS Commun.* **6** 421
[55] Jamali-Sheini F, Cheraghizade M and Yousefi R 2018 *Solid State Sci.* **79** 30
[56] Cheraghizade M, Jamali-Sheini F, Yousefi R, Niknia F, Mahmoudian M R and Sookhakian M 2017 *Mater. Chem. Phys.* **195** 187
[57] Choi Y S and Lee W I 2014 *Bull. Korean Chem. Soc.* **35** 913
[58] Kuriakose S, Satpati B and Mohapatra S 2015 *Phys. Chem. Chem. Phys.* **17** 25172
[59] Kuriakose S, Choudhary V, Satpati B and Mohapatra S 2014 *Phys. Chem. Chem. Phys.* **16** 17560
[60] Baghchesara M A, Yousefi R, Cheraghizade M, Jamali-Sheini F and Saáedi A 2016 *Cer. Int.* **42** 1891
[61] Humaira S, Kemp K C, Vimlesh C and Kwang S K 2012 *Nanotechnology* **23** 355705